Geophysical Journal International

Geophys. J. Int. (2012) **191,** 481–490 doi: 10.1111/j.1365-246X.2012.05662.x

GPS estimates of microplate motions, northern Caribbean: evidence for a Hispaniola microplate and implications for earthquake hazard

B. Benford,[1] C. DeMets[1] and E. Calais[2]

[1]*Department of Geoscience, University of Wisconsin–Madison,* 1215 *W. Dayton St., Madison, Wisconsin* 53706*, USA. E-mail: brynbenford@gmail.com*
[2]*Department of Earth and Atmospheric Sciences, Purdue University,* 550 *Stadium Mall Dr., West Lafayette, Indiana* 47906*, USA*

Accepted 2012 August 31. Received 2012 August 27; in original form 2012 April 16

SUMMARY

We use elastic block modelling of 126 GPS site velocities from Jamaica, Hispaniola, Puerto Rico and other islands in the northern Caribbean to test for the existence of a Hispaniola microplate and estimate angular velocities for the Gônave, Hispaniola, Puerto Rico-Virgin Islands and two smaller microplates relative to each other and the Caribbean and North America plates. A model in which the Gônave microplate spans the whole plate boundary between the Cayman spreading centre and Mona Passage west of Puerto Rico is rejected at a high confidence level. The data instead require an independently moving Hispaniola microplate between the Mona Passage and a likely diffuse boundary within or offshore from western Hispaniola. Our updated angular velocities predict 6.8 ± 1.0 mm yr^{-1} of left-lateral slip along the seismically hazardous Enriquillo-Plantain Garden fault zone of southwest Hispaniola, 9.8 ± 2.0 mm yr^{-1} of slip along the Septentrional fault of northern Hispaniola and ∼14–15 mm yr^{-1} of left-lateral slip along the Oriente fault south of Cuba. They also predict 5.7 ± 1 mm yr^{-1} of fault-normal motion in the vicinity of the Enriquillo-Plantain Garden fault zone, faster than previously estimated and possibly accommodated by folds and faults in the Enriquillo-Plantain Garden fault zone borderlands. Our new and a previous estimate of Gônave-Caribbean plate motion suggest that enough elastic strain accumulates to generate one to two $M_w \sim 7$ earthquakes per century along the Enriquillo-Plantain Garden and nearby faults of southwest Hispaniola. That the 2010 $M = 7.0$ Haiti earthquake ended a 240-yr-long period of seismic quiescence in this region raises concerns that it could mark the onset of a new earthquake sequence that will relieve elastic strain that has accumulated since the late 18th century.

Key words: Plate motions; Dynamics and mechanics of faulting; Neotectonics; Fractures and faults.

1 INTRODUCTION

Following the 2010 January 12 $M_w = 7.0$ Haiti earthquake (Calais *et al.* 2010; Hayes *et al.* 2010), along the southern boundary of the Gônave microplate, an international effort began to better understand the slip rates and hence seismic hazards of the numerous faults in the northern Caribbean region (e.g. Frankel *et al.* 2010; Prentice *et al.* 2010). These efforts depend critically on estimates of the present motions of microplates between the Caribbean and North America plates (Fig. 1), which in turn depend on our still-evolving understanding of the configuration and number of these microplates.

To date, the Gônave, Puerto Rico-Virgin Islands (PRVI) and south Jamaica microplates (Fig. 1) have been defined from geological, seismic and geodetic observations (Mann *et al.* 1995, 2002; Jansma & Mattioli 2005; Benford *et al.* 2012). In addition, previous authors (Byrne *et al.* 1985; Jansma *et al.* 2000; Mann *et al.* 2002) invoke a Hispaniola microplate in their discussions of the regional tectonics, but do not treat the questions of whether the Hispaniola microplate is distinct from the larger Gônave microplate and if so, where its western boundary with the Gônave microplate is located. The answers to these questions are important because accurate estimates of fault slip rates on the seismically hazardous island of Hispaniola depend critically on whether the island is part of an independent microplate or instead moves with the larger Gônave microplate.

Here, we apply elastic block modelling to an updated GPS velocity field spanning all of the Caribbean–North America plate boundary east of the Cayman spreading centre (Fig. 1b) to re-examine the configuration of microplates used by previous authors and estimate angular velocities for all the microplates along the plate boundary (Jansma *et al.* 2000; Jansma & Mattioli 2005; Manaker *et al.* 2008; Calais *et al.* 2010). In particular, we test rigorously for the existence of a distinct Hispaniola microplate and examine whether the eastern limit of the Gônave microplate coincides with the Mona Passage between Hispaniola and Puerto Rico (Figs 1 and 2; Manaker *et al.* 2008; Calais *et al.* 2010), with the topographically high and

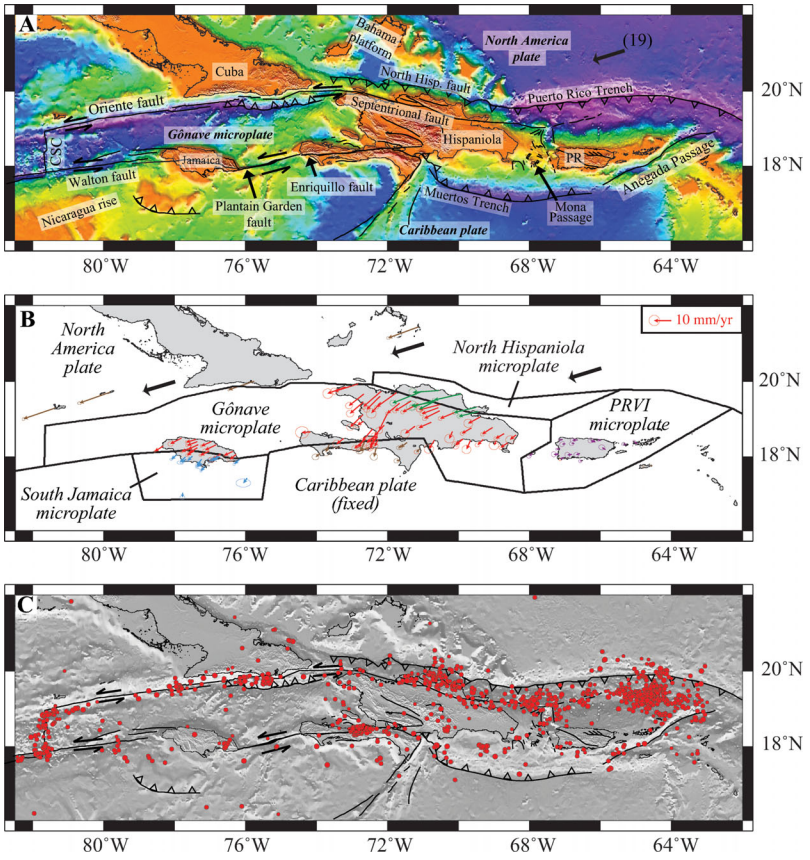

Figure 1. (a) Tectonic setting of the northern Caribbean. Bold black arrows in panels (a) and (b) show MORVEL estimate of North America plate motion in mm yr^{-1} relative to the Caribbean plate (DeMets *et al.* 2010). CSC, Cayman spreading centre; PR, Puerto Rico. Two-min seafloor bathymetry and land topography from Sandwell & Smith (1997). (b) GPS site velocities relative to Caribbean plate, with 1σ, 2-D error ellipses. Velocities from Hispaniola are taken from Calais *et al.* (2010). Velocities are colour-coded based on plate. Scale is shown in upper right corner. Black lines mark plate boundaries used for the analysis. All plates included in the analysis are labelled. PRVI microplate, Puerto Rico-Virgin Islands microplate. (c) Red circles show earthquakes from 1964–2010 (Engdahl *et al.* 1998) overlain on faults, bathymetry, and topography from (a).

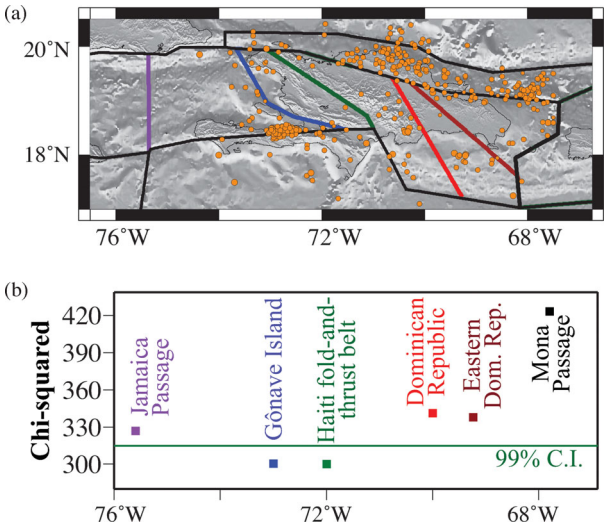

Figure 2. (a) Trial locations for the eastern boundary of the Gônave microplate shown in different colours (including the Mona Passage in black). Orange circles show 1964–2010 earthquakes (Engdahl *et al.* 1998). (b) Least-squares misfits (χ^2) for trial boundaries shown in (a). Boundary locations with misfits above the green line are excluded at the 99 per cent confidence level.

seismically active Haiti fold-and-thrust belt of central and western Hispaniola (Mann *et al.* 1995; Pubellier *et al.* 2000; Mann *et al.* 2002; Figs 1c and 3) or is located even farther west in the Jamaica Passage (Fig. 2). The new set of angular velocities defined by our analysis provides a useful basis for determining long-term fault slip rates and hence seismic hazard in this earthquake-prone region.

2 TECTONIC SETTING AND MICROPLATE CONFIGURATION

Along the Greater Antilles islands of Puerto Rico, Hispaniola and Jamaica (Fig. 1), motion between the Caribbean and North America plates is dominated by obliquely convergent, left-lateral slip at rates of 19–20 mm yr^{-1} (Dixon *et al.* 1998; DeMets *et al.* 2000, 2007; Lopez *et al.* 2006; DeMets *et al.* 2010). From east to west, the Puerto Rico trench and north Hispaniola and Oriente faults define the southern boundary of the North America plate (Fig. 1), and the Muertos Trough and Enriquillo-Plantain Garden fault zone and Walton fault define the northern boundary of the Caribbean plate (Heubeck *et al.* 1990; Mann *et al.* 1991; Rosencrantz & Mann 1991; Mann *et al.* 1995; Fig. 1). Between these two boundaries, four distinct microplates have been identified. The PRVI microplate defined by Byrne *et al.* (1985) and Masson & Scanlon (1991) moves roughly westward at 2.6 ± 2.0 mm yr^{-1} relative to the Caribbean plate interior (Jansma *et al.* 2000; Jansma & Mattioli 2005). The Gônave microplate, first proposed by Rosencrantz & Mann (1991),

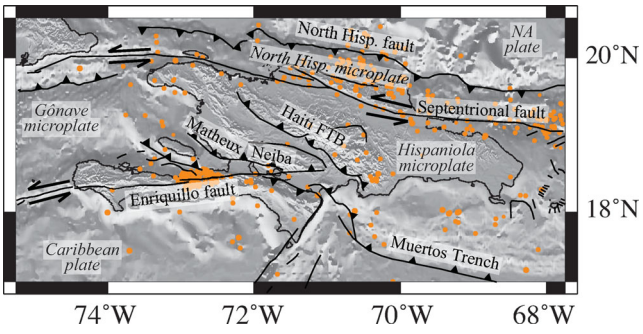

Figure 3. Major faults of Hispaniola (Mann *et al.* 1984; Pubellier *et al.* 2000; Calais *et al.* 2010) overlain on 2-min seafloor bathymetry and land topography from Sandwell & Smith (1997). Haiti FTB, Haiti fold-and-thrust belt; Matheux Neiba, Matheux Neiba fault zone; NA plate, North America plate; North Hisp. Fault, North Hispaniola fault.

moves westward at a more rapid 6–8 mm yr^{-1} (DeMets & Wiggins-Grandison 2007; Benford *et al.* 2012), also relative to the Caribbean plate. The Hispaniola block defined by Byrne *et al.* (1985) and Manaker *et al.* (2008) occupies the eastern end of the Gônave microplate and as described below is a key subject of this paper. Finally, two smaller microplates, the south Jamaica (Benford *et al.* 2012) and north Hispaniola microplates (Manaker *et al.* 2008), also appear to partition deformation along the plate boundary (Fig. 1) and are used for this analysis.

The forces responsible for moving these microplates are incompletely understood, but almost surely change along strike given the irregular geometry of the plate boundary and its well-described transition from oblique, steep-angle subduction along the Puerto Rico Trench to shear-dominated deformation in Hispaniola and locations farther west (Calais *et al.* 1992). The prominent restraining bend where the Bahama platform collides obliquely with the north edge of Hispaniola (Mann *et al.* 1995, 2002) and a smaller restraining bend where the Nicaragua Rise collides obliquely with southern Jamaica (Benford *et al.* 2012) are both associated with distributed seismicity and deformation within the Gônave microplate and are likely to be responsible for some of the slip partitioning and microplate fragmentation characteristic of the plate boundary.

3 DATA AND METHODOLOGY

The 126 GPS velocities used for this analysis (Fig. 1b and the Supporting Information section) consist of 30 velocities from Jamaica (Benford *et al.* 2012), 63 from Hispaniola (Calais *et al.* 2010), 17 from the PRVI microplate, 6 from smaller islands scattered along the North America-Caribbean plate boundary and 10 from other locations on the Caribbean plate. Processing of the raw GPS data from Hispaniola is described by Calais *et al.* (2010) and employs ITRF05. Processing of the raw data from other locations is described by Benford *et al.* (2012) and employs ITRF08. We used the Caribbean-ITRF05 angular velocity from DeMets *et al.* (2010) and a Caribbean-ITRF08 angular velocity (Table 1) to transform the respective sets of GPS velocities to a Caribbean plate reference frame.

All the GPS velocities we use are interseismic and hence include both a steady long-term component associated with the rotation of a corresponding microplate and an elastic component associated with one or more nearby active faults (Manaker *et al.* 2008). Modelling that allows for elastic, rotating blocks is thus required to separate and estimate the two effects (McCaffrey 2002; Meade & Loveless 2009). We model the GPS velocity field using the Blocks software of Meade & Loveless (2009), which treats the crust as an elastic homogeneous half-space consisting of rotating plates that are fully locked along the faults that define their boundaries. The output of

Table 1. Angular velocities from Blocks software inversion using the geometry shown in Fig. 4(c).

Plate pair	Angular velocity[a]			Ellipse axes		Azimuth	Rotation	Variances (σ_{xx}, σ_{yy}, σ_{zz}) and covariances (σ_{xy}, σ_{xz}, σ_{yz})[b]					
							uncertainty	10^{-8} radian^2/Myr^2					
	Lat.	Long.	ω	Major	Minor	of major							
	°N	°E	°/Myr	°	°	axis	°/Myr	σ_{xx}	σ_{xy}	σ_{xz}	σ_{yy}	σ_{yz}	σ_{zz}
GV-CA	−24.5	100.1	0.526	1.4	0.6	26.32	0.069	7.64	−30.35	10.17	127.67	−42.53	14.51
HI-CA	15.5	−67.5	0.809	1.0	0.4	321.67	0.129	53.66	−146.04	52.52	401.93	−144.34	52.23
NA-CA	−73.8	21.0	0.192	5.6	1.2	85.8	0.004	0.48	−1.08	0.30	5.13	−1.25	0.50
PR-CA	17.1	−67.1	0.524	0.7	0.5	41.16	0.144	87.90	−205.23	73.35	482.26	−171.95	61.65
GV-NA	−4.1	106.5	0.473	2.9	0.6	9.77	0.065	7.69	−28.80	9.87	114.94	−39.34	13.58
HI-NA	27.2	−71.5	0.877	1.8	0.3	348.33	0.127	54.44	−146.11	52.70	395.92	−142.86	51.73
PR-NA	34.0	−73.2	0.605	5.4	0.4	337.34	0.135	86.42	−198.31	71.43	456.84	−164.48	59.35
HI-GV	19.1	−72.2	1.325	0.5	0.2	272.35	0.135	54.19	−152.21	54.56	443.39	−158.26	56.82
HI-PR	12.6	−68.3	0.286	5.2	2.0	1.3	0.177	122.58	−300.82	108.50	748.45	−269.89	97.63
CA-ITRF08[c]	37.3	−100.6	0.247	2.9	0.9	302.83	0.013	0.79	−1.75	0.50	6.04	−1.81	0.76
CA-ITRF08[d]	37.7	−101.0	0.243	2.9	0.9	302.83	0.013	0.79	−1.75	0.50	6.04	−1.81	0.76
GV-ITRF08	−12.7	113.2	0.315	3.2	0.5	56.58	0.066	8.01	−29.47	10.07	115.85	−39.90	13.84
HI-ITRF08	21.1	−74.0	1.014	0.9	0.1	299.21	0.128	54.75	−146.78	52.91	396.83	−143.42	51.99
JA-ITRF08	22.0	−80.7	0.982	1.5	0.2	319.02	0.193	51.59	−224.88	74.41	989.52	−327.69	108.68
NA-ITRF08	−11.9	−85.6	0.174	2.2	0.6	30.5	0.005	0.31	−0.67	0.20	0.91	−0.56	0.26
NH-ITRF08	13.1	−79.7	0.514	15.0	1.4	53.83	0.495	777.88	−2177.57	812.63	6122.59	−2284.11	854.06
PR-ITRF08	24.3	−76.3	0.734	3.0	0.1	301.34	0.138	86.73	−198.98	71.63	457.75	−165.04	59.61

[a]Angular velocities describe counter-clockwise rotation of the first plate/block relative to the second plate. Plate abbreviations are: CA, Caribbean; GV, Gônave; HI, Hispaniola; JA, South Jamaica; NA, North America; PR, Puerto Rico-Virgin Islands. Ellipse axes are semi-major and semi-minor.
[b]Covariances are Cartesian and propagated from data uncertainties. Elements σ_{xx}, σ_{yy} and σ_{zz} are the variances of the (0°N, 0°E), (0°N, 90°E) and 90°N components of the angular velocity.
[c]Derived assuming no motion relative to Earth's centre of mass.
[d]Derived from an inversion of 12 Caribbean plate GPS site velocities corrected for assumed motions of $V_x = 0.3$, $V_y = 0.0$ and $V_z = 1.2$ mm yr^{-1} for ITRF2008 relative to Earth's centre of mass. The assumed motions are the same as for ITRF2005 relative to Earth's centre of mass (Argus 2007).

each velocity field inversion includes one angular velocity per plate (unless the plate angular velocity is specified as a model constraint), the goodness-of-fit as measured by the summed, weighted least-squares misfit χ^2, long-term slip rates parallel and orthogonal to each plate-boundary fault and elastic deformation components at each GPS site.

Three assumptions are required about faults for our modelling: their locking depths, their dips and their degree of frictional coupling. Here, we assign a uniform fault-locking depth of 15 km, but also evaluate model results for locking depths as shallow as 10 km and as deep as 20 km. For faults common between our own analysis and that of Manaker *et al.* (2008), we use the same fault dips as adopted by Manaker *et al.* For other faults, we assign dips of 90° for strike-slip faults, 60° for high-angle reverse faults and 15° or 30° for thrust faults.

We assume complete and uniform interseismic coupling across all block boundary faults, thereby maximizing the elastic deformation component everywhere in our model. This approach differs modestly from that adopted by Manaker *et al.* (2008), who assign full coupling to most faults in their model and estimate variations in coupling along the Puerto Rico and Lesser Antilles trenches. Given the remoteness of these features from much of our study area and uncertainties in those coupling estimates, variations in coupling along those features are unlikely to significantly influence our model results and are ignored hereafter.

For the analysis below, we vary only the assumed location of the eastern boundary of the Gônave microplate. The boundaries of the Gônave microplate at most other locations are well defined, as are the boundaries of the Caribbean, North America and PRVI plates. The geometry of the southern boundary of the Gônave microplate in Jamaica is constrained by GPS and geological observations (Benford *et al.* 2012). We use the MORVEL Caribbean–North America angular velocity (73.9° S, 32.6° E, 0.190° Myr^{-1}; DeMets *et al.* 2010) to tie the North America plate to the Blocks model. Estimates of fault slip rates and boundary geometries for Hispaniola are insensitive to alternative assumed geometries for the Gônave microplate boundary in Jamaica.

Finally, a general limitation of our models is the requirement that plate boundaries be narrow, discrete features. For example, deformation may be distributed across a ∼100-km-wide zone in central and western Hispaniola, where we and other authors postulate the existence of a plate boundary (Jansma *et al.* 2000; Jansma & Mattioli 2005; van Benthem & Govers 2010). Similarly, deformation in southwest Haiti may be partitioned between the strike-slip Enriquillo-Plantain Garden fault zone and nearby structures (Calais *et al.* 2010).

4 TEST FOR GEOMETRY AND EXISTENCE OF THE HISPANIOLA MICROPLATE

If the Gônave microplate extends from the Cayman spreading centre in the west (Fig. 1) to the Mona Passage between Hispaniola and Puerto Rico, it includes much of Hispaniola and Jamaica, the two major landmasses on the largely submarine Gônave microplate. If this geometry is correct, then the GPS velocities for sites in areas of Hispaniola and from the island of Jamaica should be consistent with rotation about a single angular velocity after accounting for the elastic deformation from locked plate-boundary faults. Alternatively, motion between independently moving Hispaniola and Gônave microplates would be manifested as an inconsistency between velocities recorded by sites in Jamaica and Hispaniola relative to the velocities predicted by a single angular velocity.

We test for an independent Hispaniola microplate by comparing the fit of a five-microplate model that excludes a Hispaniola microplate to the fits of several six-microplate models in which we vary the assumed locations for the Gônave-Hispaniola microplate boundary (locations indicated by the coloured lines in Fig. 2a). For each assumed geometry, we invert all 126 GPS velocities (Fig. 2) using Blocks to estimate each microplate angular velocity and the elastic effects of the faults that bound the microplates. The goodness-of-fit for each assumed boundary location is given by chi-squared (χ^2) from the Blocks inversion (Fig. 2), where χ^2 is the weighted, summed least-squares misfit. Lower values of χ^2 correspond to a better fit of the GPS velocities for a given boundary location. Angular velocities are estimated for the Caribbean, Gônave, north Hispaniola, PRVI and south Jamaica microplates; models that also include a Hispaniola microplate have three additional adjustable parameters (one angular velocity). We use the Stein & Gordon (1984) F-ratio test to evaluate the improvements in fit of the more complex six-plate models relative to the five-plate model; the F-ratio test is well suited for this analysis given its inherent insensitivity to incompletely known data uncertainties.

Fig. 2 shows the goodness-of-fit to all 252 GPS velocity components for all the models we tested. The worst fitting model, with $\chi^2 = 423.3$ (Fig. 2b), corresponds to the five-plate model, which excludes the Hispaniola microplate. In this model, the Gônave microplate extends east to the Mona Passage and thus includes all of Hispaniola and much of Jamaica. This model significantly misfits GPS velocities in both western and eastern Hispaniola (Fig. 4a), indicating that the velocities from Jamaica and Hispaniola are fit poorly if forced onto the same microplate.

The fits of all of the six-plate models we tested improve on that of the five-plate model by ∼20 per cent or more (Fig. 2b), with the best fits for assumed boundaries that coincide with either the Haiti fold-and-thrust belt (green boundary in Fig. 2a) or an assumed boundary offshore from western Hispaniola (blue boundary in Fig. 2a). An assumed boundary in the Jamaica Passage (purple boundary in Fig. 2a) fits the data worse than the two best-fitting six-plate models and as described below is rejected at the 99 per cent confidence level.

The respective least-squares misfits, $\chi^2 = 300.1$ and $\chi^2 = 300.7$, for the two best-fitting models, those with assumed boundaries that coincide with the Haiti fold-and-thrust belt or just offshore from western Hispaniola (labelled 'Gônave Island' in Fig. 2a), correspond to WRMS misfits of 0.9 mm yr^{-1} and 0.8 mm yr^{-1} in the north and east velocity components. These misfits are only ∼10 per cent larger than the estimated velocity uncertainties. As shown by the small and randomly oriented residual GPS velocities in Fig. 4b, the best-fitting models eliminate the systematic misfits to the GPS velocities in western and eastern Hispaniola observed for a model without a Hispaniola microplate (Fig. 4a).

We used the Stein & Gordon (1984) F-ratio test for an additional plate to assess whether the best overall fit ($\chi^2 = 300.1$) for the assumed Haiti fold-and-thrust belt plate boundary improves significantly on that for the model that excludes the Hispaniola microplate. For the three additional degrees of freedom corresponding to the additional Hispaniola plate angular velocity, $F = 32.0$. The probability that random errors in the GPS velocities could spuriously give rise to an F-value this high is only three parts in 10^{17}. The GPS velocities thus strongly support the existence of a Hispaniola microplate, a result not previously reported in the literature.

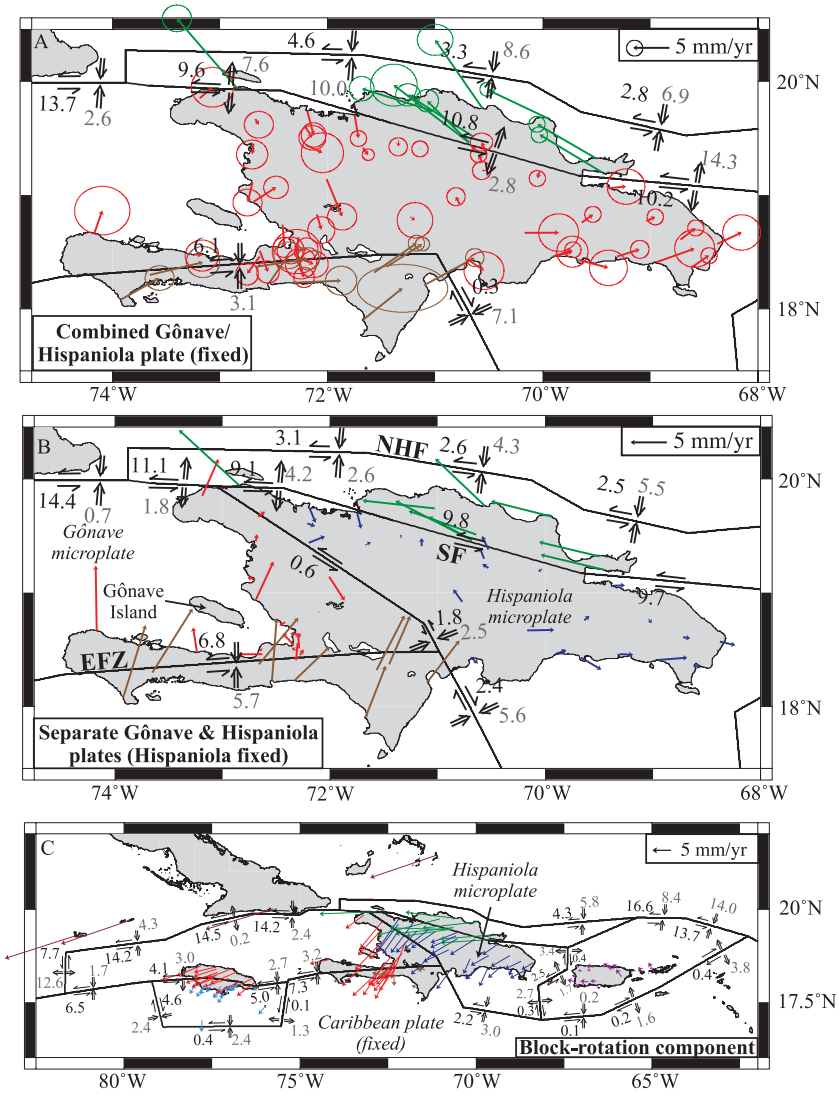

Figure 4. (a) Velocity misfits and modelled slip rates for a model that excluded an independent Hispaniola microplate. Slip rates are specified as boundary-parallel (black) and boundary-normal components (grey). Velocities are in Gônave microplate reference frame and are colour-coded per microplate. Uncertainty ellipses are 2-D, 1σ. Maximum strike-slip and convergent-slip uncertainties are 1.8 mm yr^{-1} and 2.1 mm yr^{-1}, respectively. (b) Velocity misfits and modelled slip rates for a model with an independent Hispaniola microplate. Velocities are in a Hispaniola microplate reference frame. Maximum strike-slip and convergent-slip uncertainties are 1.1 mm yr^{-1} and 1.8 mm yr^{-1}, respectively. Fault name abbreviations are: EFZ, Enriquillo-Plantain Garden fault zone; NHF, North Hispaniola fault; SF, Septentrional fault zone. (c) GPS velocities relative to Caribbean plate and corrected for elastic effects from our best-fitting Blocks model. Slip rates for Hispaniola are shown in (b). Velocities are in a Gônave microplate reference frame. Maximum strike-slip and convergent-slip uncertainties are 1.9 mm yr^{-1} for both. Scale is shown in upper right corner in all panels.

Based on a F-ratio comparison of the squared misfits for all the assumed boundary locations relative to that for the best-fitting location, assumed boundaries in the Jamaica Passage or within or east of central Hispaniola fit the data significantly worse than the two best-fitting models (Fig. 2b). We conclude that the regional GPS velocities strongly justify the addition of a Hispaniola microplate, bounded to the east by the Mona Passage and to the west by the Haiti fold-and-thrust belt or structures in far western Hispaniola (e.g. the Matheux Neiba fault zone shown in Fig. 3), including offshore faults. Although our block modelling requires plate boundaries to be discrete, the seismicity and topography in western Hispaniola are distributed and may define a diffuse plate boundary that spans the faults listed above (shown by the hachured region in Fig. 5).

We tested the degree to which the 30 GPS site velocities from Jamaica influence the above results by repeating all the above inversions while excluding those velocities (thereby eliminating nearly all the GPS sites assumed to be on the Gônave microplate). The improvement in fit for an additional Hispaniola microplate gives $F = 6.8$, which is significant at the 99 per cent confidence level (or two parts in 10^4). The kinematic evidence for a distinct Hispaniola microplate is thus weaker, but still significant if we exclude data from Jamaica that help determine the Gônave microplate angular velocity.

5 MICROPLATE ANGULAR VELOCITIES AND PREDICTED FAULT SLIP RATES

Table 1 lists the best-fitting angular velocities for the microplates in our study area relative to each other and relative to ITRF08 based on the best-fitting Gônave-Hispaniola microplate boundary that

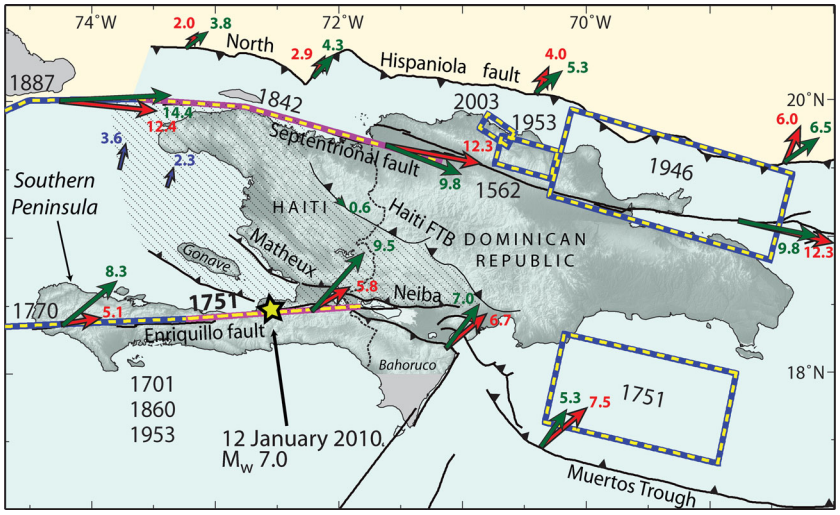

Figure 5. Comparison of plate velocities estimated herein (green arrows) and by Calais *et al.* (2010) (red arrows). Velocities shown in green are predicted from the best-fitting microplate angular velocities in Table 1 and are for an assumed Gônave-Hispaniola boundary that coincides with the Haiti fold-and-thrust belt. Blue arrows west of Hispaniola indicate motion of the Gônave microplate relative to the Hispaniola microplate for an assumed plate boundary just west of Hispaniola (indicated by blue line in Fig. 2a). Plate velocities show motion of microplate located south of the plate boundary with respect to that north of the boundary. Long-term fault slip rates derived from GPS inversions are given in mm yr^{-1}. Estimated historical rupture areas are derived from archives (McCann 2006). 1701, 1860, and 1953 are the dates of smaller magnitude, poorly located earthquakes. Presumed vertical strike-slip earthquakes are shown as lines; presumed dip-slip events are shown as projected surface areas. Hachured area may approximate the diffuse Gônave-Hispaniola plate boundary. Modified from Fig. 1 of Calais *et al.* (2010).

corresponds to the Haiti fold-and-thrust belt (Fig. 2a). The formal angular velocity covariances estimated from Blocks (Table 1) are likely to be too small because they are based on the simplifying assumptions that the fault locking depths, fault dips and microplate geometries are well known, that full coupling occurs across all faults, and that the microplate boundaries are discrete. To better understand some of the modelling trade-offs and hence estimate more realistic uncertainties, we derived models using a variety of alternative microplate geometries, different subsets of the GPS velocity field, different geologically plausible constraints for the slip type along particular faults and fault locking depths as shallow as 10 km and as deep as 20 km. The uncertainties stated below, which are based on these sensitivity tests, are typically larger than the formal uncertainties by a factor of two to three and approximate the 95 per cent confidence limits.

5.1 Septentrional fault

The complexly deforming island of Hispaniola includes the seismically hazardous Septentrional and Enriquillo-Plantain Garden faults (Fig. 5), as well as seismically active faults in offshore areas around the island (Figs 1 and 2a). Left-lateral slip of 9.8 ± 2 mm yr^{-1} is predicted for the Septentrional fault (Figs 4b and 5), near the middle of the 6–12 mm yr^{-1} geologically estimated slip rate for the fault (Prentice *et al.* 2003) and modestly slower than but consistent with the 12 ± 2 mm yr^{-1} rate estimated by Calais *et al.* (2010) from GPS velocity block modelling with DEFNODE software (McCaffrey 2002). Sensitivity tests in which we vary the factors described in the preceding paragraph suggest a 13 mm yr^{-1} maximum slip rate for this fault.

5.2 Enriquillo-Plantain garden fault zone

The Gônave-Caribbean angular velocity (Table 1) predicts 8–9.5 mm yr^{-1} of obliquely convergent slip along the Enriquillo-Plantain Garden fault zone of western Haiti (Fig. 5). For comparison, Calais *et al.* (2010) estimate motion of 5.1–5.8 mm yr^{-1} from their inversion of GPS velocities solely from Hispaniola (Fig. 5). Our revised estimate is thus faster than and more oblique to the fault than that of Calais *et al.* At a central point along the N85°E-striking fault, our newly predicted Gônave-Caribbean plate velocity resolves into 6.8 ± 1 mm yr^{-1} of fault-parallel left-lateral slip and 5.7 ± 1 mm yr^{-1} of boundary-normal convergence (Fig. 4b). For comparison, the velocity estimated by Calais *et al.* (2010) resolves into 5 ± 1 mm yr^{-1} of fault-parallel and 2 ± 1 mm yr^{-1} of fault-normal motion. Our respective fault-parallel rate estimates are therefore consistent within their estimated uncertainties. In contrast, our model predicts fault-normal convergence that is a factor of three faster (5.7 mm yr^{-1} versus 2 mm yr^{-1}) than predicted by Calais *et al.*'s model.

Most of the difference in the predictions of the two models is caused by the different Gônave microplate geometries used in our two studies and the new GPS velocities from northern Jamaica that we use to constrain motion of the Gônave microplate (Fig. 1 and Benford *et al.* 2012). The Gônave-Caribbean plate angular velocity for our five-plate model, which simulates the microplate geometries assumed by Calais *et al.* (2010), predicts a fault-normal convergent component along the Enriquillo-Plantain Garden fault zone of only 3.1 ± 1 mm yr^{-1}, close to that (2 mm yr^{-1}) predicted by Calais *et al.* However, as described above, this sub-optimal microplate geometry increases the misfit by more than 30 per cent (Fig. 2b) and is rejected at high confidence level.

The more rapid convergence predicted by our model for the Gônave-Caribbean plate boundary in southwest Hispaniola poses a conundrum given that geological and seismic evidence indicate that the primary plate boundary structure, the Enriquillo-Plantain Garden fault zone, is a strike-slip fault. We thus postulate that the oblique convergence predicted by our model is partitioned onto the Enriquillo-Plantain Garden fault zone and structures north and possibly south of the fault zone. Mann *et al.* (1995) describes underwater folds and reverse faults north of Haiti's southwest peninsula

that could play a role in the postulated partitioning. The 2010 Haiti earthquake, which occurred on a buried fault close to, but north of the Enriquillo-Plantain Garden fault zone, accommodated 2.6 m of slip parallel to and 1.8 m of slip orthogonal to the Enriquillo-Plantain Garden fault zone (Calais *et al.* 2010). The nearly 40 per cent reverse dip-slip component for this earthquake and predominance of thrust-faulting aftershocks following the earthquake (Nettles & Hjörleifsdóttir 2010; Mercier de Lépinay *et al.* 2011) are both strong evidence for a significant component of boundary-normal convergence, as predicted by our model.

We tested the robustness of our model velocity estimates for the Enriquillo-Plantain Garden fault zone by re-inverting the GPS velocity field while imposing the following constraints on the outcomes of our velocity field inversions: (1) pure strike-slip motion was required along the Enriquillo-Plantain Garden fault zone, (2) pure strike-slip motion was required along the Oriente fault west of Cuba (Fig. 1), (3) pure strike-slip motion was enforced across both the Oriente and Walton faults west of Jamaica (Fig. 1) and (4) various subsets of GPS velocities on the Gônave microplate were excluded. Enforcing the first constraint increases the model misfit ∼30 per cent and is rejected at high confidence level. For cases (2) through (4), the estimated slip rate component parallel to the Enriquillo-Plantain Garden fault zone differs by no more than 0.6 mm yr^{-1} from our best-fitting estimate of 6.8 mm yr^{-1}. Cases 2 and 3 reduce the estimated convergent slip rate component orthogonal to the Enriquillo-Plantain Garden fault zone to 4.5–4.8 mm yr^{-1}, slower than the 5.7 mm yr^{-1} best estimate, but still faster than the 2 ± 1 mm yr^{-1} estimated by Calais *et al.* (2010). Case 4 variously changes the boundary normal rate component to 5.3–6.2 mm yr^{-1}. We conclude that the rate of strike-slip motion in western Hispaniola is well determined and that the faster-than-expected convergent component of Gônave-Caribbean plate motion in western Haiti is a robust feature of our data and modelling.

5.3 Hispaniola-Gônave microplate motion: slow convergence in western Hispaniola

The Hispaniola-Gônave rotation pole is located in western Hispaniola and remains nearly fixed whether we adopt the boundary just west of Hispaniola or a boundary that coincides with the Haiti fold-and-thrust belt. Surprisingly, the best-fitting angular velocity (Table 1), located in western Hispaniola at 19.1°N, 72.2°W, predicts that almost no deformation occurs across the Haiti fold-and-thrust belt (Figs 4b, c and 5). For example, at a central location in the fold-and-thrust belt, it predicts NW-directed dextral shear of only 0.6 ± 1.5 mm yr^{-1}. If we instead assume the plate boundary is located just west of the island, the resulting Hispaniola-Gônave angular velocity (19.1°N, 72.4°W, 1.30° Myr^{-1}) predicts oblique convergence at rates of 2.3–3.6 mm yr^{-1} across the NW- to WNW-oriented reverse faults in western Haiti and offshore (Fig. 5).

Although the predicted slow deformation across the Hispaniola-Gônave plate boundary seems at odds with the kinematic evidence for significant motion between the two microplates, we reiterate that the latter is a consequence of the previously described inconsistency between the GPS site velocities from Jamaica and eastern Hispaniola (Fig. 4a). Direct seismologic or geological evidence for the slow deformation is weak, partly because of the difficulty in finding clear geomorphologic evidence of slowly slipping faults in rapidly eroding tropical terrains. Earthquakes in central and western Hispaniola in 1761, 1775, 1793 and 1911 may indicate the existence of a diffuse plate boundary in western Hispaniola, but the earthquake locations and magnitudes are uncertain (Woodring *et al.* 1924). At minimum, observations needed to better understand the kinematics of this likely diffuse plate boundary might include more and better determined GPS site velocities from western Hispaniola and detailed maps of active Quaternary deformation both offshore from western Hispaniola and within western Hispaniola.

5.4 Oriente fault

The new angular velocities predict that Caribbean–North America plate motion is partitioned into 14.2–14.5 (±1) mm yr^{-1} of left-lateral slip along the Oriente fault south and west of Cuba and 4.1–7.3 (±1) mm yr^{-1} of left-lateral slip along faults that define the southern edge of the Gônave microplate (Figs 1, 4c and 5). The latter agrees with a 3–7 mm yr^{-1} geological estimate based on post-9 Myr fault offsets in eastern Jamaica and the Jamaica Passage (Natural Disaster Research 1999), and supersedes a somewhat faster 8 mm yr^{-1} estimate of the minimum slip rate based on an earlier velocity field from Jamaica (DeMets & Wiggins-Grandison 2007).

5.5 Cayman spreading centre

The best-fitting Gônave-North America angular velocity (Table 1) predicts a 12.6 ± 0.6 mm yr^{-1} seafloor-spreading rate across the Cayman spreading centre (Fig. 4c). Long-term opening rates based on Cayman spreading centre magnetic anomalies (Macdonald & Holcombe 1978; Leroy *et al.* 2000) and on seafloor depth and seafloor age profiles (Rosencrantz *et al.* 1988) range between 12 and 20 mm yr^{-1}. DeMets & Wiggins-Grandison (2007) estimate a 6–11 mm yr^{-1} short-term opening rate based on geodetic results from Jamaica. The modestly faster rate predicted by our new model is more consistent with the estimated long-term opening rate.

6 DISCUSSION: SEISMIC HAZARD AND DRIVING FORCES

6.1 Seismic hazard

Our work implies greater earthquake hazard along the Enriquillo-Plantain Garden fault zone of southwestern Haiti than previous studies. The 6.8 ± 1 mm yr^{-1} of fault-parallel left-lateral slip predicted by our best model agrees with prior estimates within uncertainties (Dixon *et al.* 1998; Calais *et al.* 2002; Mann *et al.* 2002; Manaker *et al.* 2008; Calais *et al.* 2010). However, the 5.7 ± 1 mm yr^{-1} of boundary-normal convergence predicted by our model is a factor of 3 greater than estimated by Calais *et al.* (2010). Given that the surprisingly rapid estimated fault-normal component of motion is robust with respect to a variety of sensitivity tests and that the 2010 Haiti earthquake included a reverse slip component equal to nearly 40 per cent of the seismic moment (Calais *et al.* 2010), partitioning of the oblique plate motion onto separate sets of faults may occur.

If the Enriquillo-Plantain Garden fault zone accommodates all of the boundary-parallel component of motion, which appears likely given the evidence it has ruptured multiple times in the late Quaternary (Prentice *et al.* 2010), our best model predicts that the fault accrues a 0.68 ± 0.1 m slip deficit per century. Simple calculations show that it takes ∼600 years for a 30-km-long by 10-km-deep fault, approximately the rupture dimensions of the 2010 Haiti earthquake (Calais *et al.* 2010), to accumulate enough seismic moment at the predicted slip rate to produce a $M_w = 7.0$ earthquake. For the

300-km-long Enriquillo-Plantain Garden fault zone, the accumulated seismic moment deficit is therefore large enough to cause one $M_w \sim 7$ strike-slip earthquake every 60 years on a ∼30-km-long segment somewhere along the fault. For comparison, the 5–6 mm yr^{-1} fault-parallel slip rate predicted by Calais *et al.* (2010) predicts a modestly longer 75–90 yr recurrence interval for a $M_w \sim 7$ strike-slip earthquake somewhere along the fault.

Unlike the kinematic model described by Calais *et al.* (2010), which predicts a relatively small 2 ± 1 mm yr^{-1} component of motion orthogonal to the Enriquillo-Plantain Garden fault zone, our model predicts that a fault-normal slip deficit accrues at 0.57 ± 0.1 m per century. Assuming 60° dips for assumed reverse-slip faults that extend along the 300-km-long boundary and repeating the calculations above for assumed 30-km-long locked segments, we find that enough sufficient seismic moment accumulates to generate one $M_w \sim 7$ reverse-slip earthquake every 60–70 yr.

The rates of strain accumulation determined from the above kinematic models therefore imply that between one and two Mw∼7 earthquakes could occur per century somewhere along the Gônave-Caribbean plate boundary in southern Haiti. For comparison, only four $M_w \sim 7$ earthquakes occurred in southern Haiti between 1500 and 2009, one in 1701 ($M_I = 6.6$), two in 1751 ($M_I = 7.4$–7.5 and $M_I = 6.6$) and one in 1770 ($M_I = 6.6$; Scherer 1912; Bakun *et al.* 2012). The 18th century earthquake cluster and long quiescent periods before and after those clustered earthquakes raises concerns that the 2010 $M = 7.0$ Haiti earthquake may initiate a sequence of $M \sim 7$ earthquakes that relieve the elastic strain that has accumulated during the past few centuries (Bakun *et al.* 2012). Alternatively, some or all of the accumulated strain might be relieved by fewer but larger magnitude earthquakes or aseismic processes such as creep along active faults or plastic deformation (e.g. folding, as observed offshore; Bien-Aime Momplaisir 1986). Additional research on the palaeo-earthquake record may help discriminate between these hypotheses.

6.2 Driving forces

Our kinematic model offers intriguing new clues about the forces that influence microplate motions along the shear-dominated Caribbean–North America plate boundary. Slow CCW rotation of the PRVI microplate about a pole immediately south of the microplate (Table 1), giving rise to 1–1.5 mm yr^{-1} of dominantly westward PRVI motion relative to the Caribbean plate, may be driven by oblique left-lateral shear across the plate boundary. Our kinematic results strongly support those reported earlier by Jansma *et al.* (2000) and Jansma & Mattioli (2005), who report GPS evidence for 2.5 ± 2 mm yr^{-1} of dominantly westward PRVI motion.

Masson & Scanlon (1991) propose that the PRVI microplate rotates slowly CCW and translates slowly to the west along the Puerto Rico Trench, consistent with their interpretation of long-range sidescan sonar data and seismic reflection profiles near Puerto Rico. Our kinematic results strongly support their conclusions. An earlier proposal by Jany *et al.* (1987) for eastward tectonic 'escape' of the PRVI block conflicts with GPS measurements later reported by Jansma *et al.* (2000) and Jansma & Mattioli (2005), who find westward rather than eastward motion of the PRVI microplate. Our model results also demonstrate slow westward motion of PRVI, as found by Jansma *et al.* (2000) and Jansma & Mattioli (2005).

The more rapid CCW rotation of the Hispaniola microplate than the PRVI microplate is presumably driven by oblique collision of the Bahama platform with north-central Hispaniola (Mann *et al.* 1995, 2002). The effects of the collision are profound and include rifting in the Mona Passage and a distinct change from westward motion in western Puerto Rico to S–W motion in eastern Hispaniola (Figs 1b and 4c). From forward modelling of the forces and hence torques that act on the Caribbean plate and comparisons to the observed regional stresses, vertical-axis rotations and earthquake slip directions, van Benthem & Govers (2010) conclude that microplates in the northeast Caribbean should rotate CCW. This agrees with our Caribbean-fixed angular velocities of the Hispaniola and PRVI microplates (Table 1), which predict slow CCW rotations for both microplates.

Our model also includes the first estimate of Gônave microplate angular velocities. Contrary to the CCW rotations of the Hispaniola and PRVI microplates, the Gônave microplate rotates slowly CW (Fig. 4c). The estimated CW rotation agrees with the slow CW rotation predicted by van Benthem & Govers (2010) for the Gônave microplate. Its opposite-sense rotation may be caused by two factors, namely, the southward push on the eastern end of the Gônave microplate from rapid CCW rotation of the Hispaniola microplate (Fig. 4c) and oblique convergence of the Nicaragua Rise with the southern boundary of the Gônave microplate, which may pin and hence create a pivot point for the microplate or push it northward (Fig. 1). The Gônave microplate is elongate subparallel to the direction of plate motion and is thus unlikely to rotate rapidly in response to shear imposed along its northern and southern boundaries (Lamb 1994).

7 CONCLUSION

GPS site velocities from the two largest islands potentially on the Gônave microplate, Hispaniola and Jamaica, are fit poorly by a single angular velocity when the site velocities are corrected for interseismic elastic deformation from faults locked along the microplate boundaries. In particular, the velocities of sites in eastern Hispaniola are misfit systematically and significantly when inverted simultaneously with well-defined velocities from sites on parts of Jamaica and western Hispaniola that lie on the Gônave microplate. A discrete or diffuse boundary between the Gônave and Hispaniola microplates thus lies between eastern Hispaniola and Jamaica. Inversions of the 126 velocities from GPS sites along the Caribbean–North America plate boundary for a range of assumed Gônave-Hispaniola boundary locations indicate that the boundary is most likely located in central or western Haiti, coinciding with the Haiti fold-and-thrust belt or offshore faults west of Hispaniola.

An inversion of the regional GPS site velocities using the newly defined Hispaniola microplate, as well as the Gônave, north Hispaniola, south Jamaica and PRVI microplates gives new angular velocities for these microplates relative to each other and relative to the Caribbean and North America plates and ITRF2008. These angular velocities and their uncertainties provide a useful new basis for studies of the regional-scale deformation, as well as seismic hazard for specific plate-boundary faults. Our new estimate and an estimate previously published by Calais *et al.* (2010) for Gônave-Caribbean plate motion show that the Enriquillo-Plantain Garden fault zone and nearby faults of southwest Hispaniola accumulate elastic strain at a rate equivalent, on average, to one to two $M_w \sim 7$ earthquakes per century. Evidence for temporally clustered $M \sim 7$ earthquakes in southern Hispaniola during the 18th century (Bakun *et al.* 2012) raises concerns that the 2010 $M = 7.0$ Haiti earthquake could mark the onset of a new earthquake sequence that will relieve elastic strain that has accumulated since the late 18th century.

ACKNOWLEDGMENTS

This project was funded by National Science Foundation grant EAR-0609578. Some of this material is based on data provided by the UNAVCO Facility with support from the National Science Foundation (NSF) and National Aeronautics and Space Administration (NASA) under NSF Cooperative Agreement No. EAR-0735156. Figures were produced using Generic Mapping Tools software (Wessel & Smith 1991).

REFERENCES

Argus, D.F., 2007. Defining the translational velocity of the reference frame of Earth, *Geophys. J. Int.,* **169,** 830–838, doi:10.1111j.1365-246X.2007.03344.x.

Bakun, W.H., Flores, C.H. & ten Brink, U.S., 2012. Significant earthquakes on the Enriquillo fault system, Hispaniola, 1500–2010: Implications for seismic hazard, *Bull. seism. Soc. Am.,* **102,** 18–30, doi:10.1785/0120110077.

Benford, B., DeMets, C., Tikoff, B., Williams, P., Brown, L. & Wiggins-Grandison, M., 2012. Seismic hazard along the southern boundary of the Gônave microplate: Block modeling of GPS velocities from Jamaica and nearby islands, northern Caribbean, *Geophys. J. Int.,* **190,** 59–74, doi:10.1111/j.1365-246X.2012.05493.x.

Bien-Aime Momplaisir, R., 1986. Contribution à l'étude géologique de la partie orientale du massif de la Hotte (presquîle du sud d'Haiti); Synthèse structurale des marges de las presquîle à partur de données sismiques, *PhD thesis,* Université Pierre et Marie Curie (Parvis VI), Paris, p. 210.

Byrne, D.B., Suarez, G. & McCann, W.R., 1985. Muertos Trough subduction-microplate tectonics in the northern Caribbean?, *Nature,* **317,** 420–421.

Calais, E., Béthoux, N. & Mercier de Lépinay, B., 1992. From transcurrent faulting to frontal subduction: a seismotectonic study of the northern Caribbean plate boundary from Cuba to Puerto Rico, *Tectonics,* **11,** 114–123.

Calais, E., Mazabraud, Y., Mercier de Lépinay, B., Mann, P., Mattioli, G. & Jansma, P., 2002. Oblique strain partitioning and fault slip rates in the northeastern Caribbean from GPS measurements, *Geophys. Res. Lett.,* **20,** 1856–1859, doi:10.1029/2002GL015397.

Calais, E. *et al*., 2010. Transpressional rupture of an unmapped fault during the 2010 Haiti earthquake, *Nat. Geosci.,* **3,** 794–799, doi:10.1038/NGEO992.

DeMets, C. & Wiggins-Grandison, M., 2007. Deformation of Jamaica and motion of the Gônave microplate from GPS and seismic data, *Geophys. J. Int.,* **168,** 362–378, doi:10.1111/j.1365-246X.2006.03236.x.

DeMets, C., Jansma, P.E., Mattioli, G.S., Dixon, T.H., Farina, F., Bilham, R., Calais, E. & Mann, P., 2000. GPS geodetic constraints on Caribbean-North America plate motion, *Geophys. Res. Lett.,* **27,** 437–440, doi:10.1029/1999GL005436.

DeMets, C., Mattioli, G., Jansma, P., Rogers, R.D., Tenorio, C. & Turner, H.L., 2007. Present motion and deformation of the Caribbean plate: Constraints from new GPS geodetic measurements from Honduras and Nicaragua, in *Geologic and Tectonic Development of the Caribbean Plate in Northern-Central America,* Geol. Soc. Am. Spec. Paper Vol. 428, pp. 21–36, ed. Mann, P., The Geological Society of America, Boulder, CO, doi: 10.1130/2007.2428(02).

DeMets, C., Gordon, R.G. & Argus, D.F., 2010. Geologically current plate motions, *Geophys. J. Int.,* **181,** 1–80, doi:10.1111/j.1365256X.2009.04491.x.

Dixon, T.H., Farina, F., DeMets, C., Jansma, P., Mann, P. & Calais, E., 1998. Relative motion between the Caribbean and North American plates and related boundary zone deformation from a decade of GPS observations, *J. geophys. Res.,* **103,** 15 157–15 182, doi:10.1029/97JB03575.

Engdahl, E.R., van der Hilst, R.D. & Buland, R.P., 1998. Global teleseismic earthquake relocation with improved travel times and procedures for depth determination, *Bull. seism. Soc. Am.,* **88,** 722–743.

Frankel, A., Harmsen, S., Mueller, C., Calais, E. & Haase, J., 2010. Documentation for initial seismic hazard maps for Haiti. Open-File Rep, U.S. Geol. Surv. 2010–1067, 20pp.

Hayes, G.P. *et al*., 2010. Complex rupture during the 12 January 2010 Haiti earthquake, *Nat. Geosci.,* doi:10.1038/NGEO977.

Heubeck, C., Mann, P., Dolan, J. & Monechi, S., 1990. Diachronous uplift and recycling of sedimentary basins during Cenozoic tectonic transpression, northeastern Caribbean plate margin, *Sediment. Geol.,* **70,** 1–32.

Jansma, P.E. & Mattioli, G.S., 2005. GPS results from Puerto Rico and the Virgin Islands: constraints on tectonic setting and rates of active faulting, in *Active Tectonics and Seismic Hazards of Puerto Rico, the Virgin Islands, and Offshore Areas,* Geol. Soc. Am. Spec. Paper Vol. 385, pp. 13–30, ed. Mann, P., The Geological Society of America, Boulder, CO, doi:10.1130/2007.2428(02).

Jansma, P.E., Mattioli, G.S., Lopez, A., DeMets, C., Dixon, T.H., Mann, P. & Calais E., 2000. Neotectonics of Puerto Rico and the Virgin Islands, northeastern Caribbean, from GPS geodesy, *Tectonics,* **19**(6), 1021–1037.

Jany, I., Mauffret, A., Bouysse, P., Mascle, A., Mercier de Lépinay, B., Renard, V. & Stephan, J.F., 1987. Relevé bathymétrique Seabeam et tectonique en décrochement au sud des Iles Vierges [Nord-Est Caraibes], *C.R. Acad. Sci. Paris,* **304**(Ser. II), 527–532.

Lamb, S., 1994. A model for tectonic rotations about a vertical axis, *J. geophys. Res.,* **99,** 4457–4483, doi:10.1029/93JB02574.

Leroy, S., Mauffret, A., Patriat, P. & Mercier de Lepinay, B., 2000. An alternative interpretation of the Cayman trough evolution from a reidentification of magnetic anomalies, *Geophys. J. Int.,* **141,** 539–557.

Lopez, A.M., Stein, S., Dixon, T., Sella, G., Calais, E., Jansma, P., Weber, J. & LaFemina, P., 2006. Is there a northern Lesser Antilles forearc block?, *Geophys. Res. Lett.,* **33,** L07313, doi:10.1029/2005GL025293.

Macdonald, K.C. & Holcombe, T.L., 1978. Inversion of magnetic anomalies and sea-floor spreading in the Cayman Trough, *Earth planet. Sci. Lett.,* **40,** 407–414.

Manaker, D.M. *et al*., 2008. Interseismic plate coupling and strain partitioning in the northeastern Caribbean, *Geophys. J. Int.,* **174,** 889–903, doi:10.1111/j.1365-246X.2008.03819.x.

Mann, P., Burke, K. & Matumoto, T., 1984. Neotectonics of Hispaniola: plate motion, sedimentation, and seismicity at a restraining bend, *Earth planet. Sci. Lett.,* **70,** 311–324.

Mann, P., McLaughlin, P.P. & Cooper, J.C., 1991. Geology of the Azua and Enriquillo basins, Dominican Republic; 2, Structure and Tectonics, in *Geologic and Tectonic Development of the North America-Caribbean Plate Boundary in Hispaniola,* Geol. Soc. Am. Spec. Paper Vol. 262, pp. 367–389, eds Mann, P., Draper, G. & Lewis, J.F., The Geological Society of America, Boulder, CO.

Mann, P., Taylor, F.W., Edwards, R.L. & Ku, T., 1995. Actively evolving microplate formation by oblique collision and sideways motion along strike-slip faults: an example from the northeastern Caribbean plate margin, *Tectonophysics,* **246,** 1–69.

Mann, P., Calais, E., Ruegg, J.-C., DeMets, C., Jansma, P. & Mattioli, G.S., 2002. Oblique collision in the northeastern Caribbean from GPS measurements and geological observations, *Tectonics,* **37,** doi:0.1029/2001TC001304.

Masson, D.G. & Scanlon, K.M., 1991. The neotectonic setting of Puerto Rico, *Geol. Soc. Am. Bull.,* **103,** 144–154, doi:10.1130/0016-7606(1991)103<0144:TNSOPR>2.3.CO;2.

McCaffrey, R., 2002. Crustal block rotations and plate coupling, in *Plate Boundary Zones,* Geodynamics Series, Vol. 30, pp. 101–122, eds Stein, S. & Freymueller, J.T., American Geophysical Union, Washington, D.C.

McCann, W.R., 2006. Estimating the threat of tsunamogenic earthquakes and earthquake-induced landslide tsunami in the Caribbean, in *Caribbean Tsunami Hazard, Proceedings of the NSF Caribbean Tsunami Workshop,* 2004 March 30–31, pp. 43–65, eds Mercado-Irizarry, A. & Liu, P., World Scientific Publishing Co., Singapore.

Meade, B.J. & Loveless, J.P., 2009. Block modeling with connected fault-network geometries and a linear elastic coupling estimator in spherical coordinates, *Bull. seism. Soc. Am.,* **99,** 3124–3139, doi:10.17850120090088.

Mercier de Lépinay, B. *et al*., 2011. The 2010 Haiti earthquake: a complex fault pattern constrained by seismologic and tectonic observations, *Geophys. Res. Lett.,* **38,** L22305, doi:10.1029/2011GL049799.

Natural Disaster Research, Inc., Earthquake Unit, Mines & Geology Division, 1999. Kingston metropolitan area seismic hazard assessment final report, Caribbean disaster mitigation project, Organization of American States. Available at: www.oas.org/cdmp/document/kma/seismic/kma1.htm (last accessed 2007 September), 82pp.

Nettles, M. & Hjörleifsdóttir, V., 2010. Earthquake source parameters for the 2010 January Haiti main shock and aftershock sequence, *Geophys. J. Int.,* **183,** 375–380, doi:10.1111/j.1365-246X.2010.04732.x.

Prentice, C.S., Mann, P., Peña, L.R. & Burr, G., 2003. Slip rate and earthquake recurrence along the central Septentrional fault, North American-Caribbean plate boundary, Dominican Republic, *J. geophys. Res.,* **108**(B3), 2149, doi:10.1029/2001JB000442.

Prentice, C.S., Mann, P., Crone, A.J., Gold, R.D., Hudnut, K.W., Briggs, R.W., Koehler, R.D. & Jean, P., 2010. Seismic hazard of the Enriquillo-Plantain Garden fault in Haiti inferred from palaeoseismology, *Nat. Geosci.,* **3,** 789–793, doi:10.1038/NGEO991.

Pubellier, M., Mauffret, A., Leroy, S., Vila, J.M. & Amilcar, H., 2000. Plate boundary readjustment in oblique convergence: Example of the Neogene of Hispaniola, Greater Antilles, *Tectonics,* **19,** 630–648.

Rosencrantz, E. & Mann, P., 1991. SeaMARC II mapping of transform faults in the Cayman Trough, Caribbean Sea, *Geology,* **19,** 690–693, doi:10.1130/0091-7613(1991)019<0690:SIMOTF>2.3.CO;2.

Rosencrantz, E., Ross, M. & Sclater, J., 1988. Age and spreading history of the Cayman Trough as determined from depth, heat flow, and magnetic anomalies, *J. geophys. Res.,* **93,** 2141–2157.

Sandwell, D.T. & Smith, W.H.F., 1997. Marine gravity anomaly from Geosat and ERS 1 altimetry, *J. geophys. Res.,* **102,** 10039–10054.

Scherer, J., 1912. Great earthquakes in the Island of Haiti, *Bull. seismol. Soc. Am.,* **2,** 161–180.

Stein, S. & Gordon, R.G., 1984. Statistical tests of additional plate boundaries from plate motion inversions, *Earth planet. Sci. Lett.,* **69,** 401–412.

van Benthem, S. & Govers, R., 2010. The Caribbean plate: pulled, pushed, or dragged?, *J. geophys. Res.,* **115,** B10409, doi:10.1029/2009JB006950.

Wessel, P. & Smith, W.H.F., 1991. Free software helps map and display data, *EOS, Trans. Am. Geophys. Un.,* **72,** 441–446.

Woodring, W.P., Brown, J.S. & Burbank, W.S., 1924. *Geology of the Republic of Haiti,* Department of Public Works, Lord Baltimore Press, Republic of Haiti, 631pp.

SUPPORTING INFORMATION

Additional Supporting Information may be found in the online version of this article:

Figure S1. Elastic (a) and rotational (b–d) components of GPS velocities based on best-fitting model. Scale is in upper right corner of all panels. (a) Best-fitting elastic component of GPS velocities estimated with blocks. These velocities show the elastic effects of fault locking, independent of the rotational component (b–d). (b) GPS velocities relative to Gônave microplate corrected for elastic effects shown in (a). Velocities thus illustrate rotational component of the site motions, independent of the elastic effects associated with locked faults. Scale is in upper right corner. (c) Same as B but fixed North America plate. (d) Same as (b) but fixed Hispaniola plate.

Table S1. GPS velocities with respect to the Caribbean plate.

Please note: Wiley-Blackwell are not responsible for the content or functionality of any supporting materials supplied by the authors. Any queries (other than missing material) should be directed to the corresponding author for the article.